



Water-assisted melt processing of cellulose biocomposites with poly(ϵ -caprolactone) or poly(ethylene-acrylic acid) for the production of

Downloaded from: <https://research.chalmers.se>, 2025-12-05 00:13 UTC







Citation for the original published paper (version of record):

Venkatesh, A., Forsgren, L., Avella, A. et al (2022). Water-assisted melt processing of cellulose biocomposites with poly(ϵ -caprolactone) or poly(ethylene-acrylic acid) for the production of carton screw caps. *Journal of Applied Polymer Science*, 139(6). <http://dx.doi.org/10.1002/app.51615>

N.B. When citing this work, cite the original published paper.

ARTICLE

Water-assisted melt processing of cellulose biocomposites with poly(ϵ -caprolactone) or poly(ethylene-acrylic acid) for the production of carton screw caps

Abhijit Venkatesh¹  | Lilian Forsgren¹  | Angelica Avella¹  | Karl Banke² | Jan Wahlberg³ | Fabiola Vilaseca⁴  | Giada Lo Re¹  | Antal Boldizar¹ 

¹Department of Industrial and Materials Science, Chalmers University of Technology, Gothenburg, Sweden

²Polykemi AB, Ystad, Sweden

³Tetra Pak, Lund, Sweden

⁴Department of Chemical Engineering, University of Girona, Girona, Spain

Correspondence

Abhijit Venkatesh, Department of Industrial and Materials Science, Chalmers University of Technology, SE-412 96 Gothenburg, Sweden.
Email: abhijit.venkatesh@chalmers.se

Funding information

Knut och Alice Wallenbergs Stiftelse; Stiftelsen for Strategisk Forskning; Svenska Forskningsrådet Formas

Abstract

Composites in 25 kg batches were compounded of cellulose nanocrystals (CNC) and thermomechanical pulp (TMP) and shaped into caps at industrial facilities on a pilot-plant scale. Some of the material was also injection molded into plaques to compare the effect of laboratory-scale and pilot-scale compounding of poly(ethylene-co-acrylic acid) (EAA7) and poly(caprolactone) composites reinforced with 10 wt% CNC and TMP. The materials compounded under laboratory-scale conditions showed a different morphology, improved mechanical properties, and a higher viscosity, than the materials compounded on a pilot-scale. In some cases, the rheological properties of the melts indicated the presence of a relatively strong percolating cellulosic network, and the interphase region between the cellulose and the matrix appears to be important for the mechanical performance of the composites. After the compounding on a pilot scale, both the length and width of the pulp fibers was reduced. The TMP provided better reinforcement than the CNC possibly due to the higher aspect ratio.

KEYWORDS

cellulose and other wood products, composites, mechanical properties, manufacturing, thermoplastics

1 | INTRODUCTION

The search for more sustainable solutions for plastics¹ has led to an interest in the use of cellulose as a reinforcement in polymer composites. Various types of cellulose originating from different sources and having different compositions have been used as fillers or reinforcement for decades, due to their renewability, biodegradability, abundance and interesting mechanical properties,^{2,3} and cellulose nanocrystals (CNC) now open up new

possibilities of producing renewable highly stiff composites.^{4,5} A major concern, however, is the poor compatibility between the hydrophilic cellulose and, often, hydrophobic polymer, leading to poor adhesion and poor dispersion of the cellulose in the matrix and thus a poor reinforcing effect.^{6,7} Several studies show that the mechanical properties of the final composite strongly depend not only on the cellulose source and grade but also on the effect of the processing parameters on the dispersion and homogeneity of the material.^{6,8}

This is an open access article under the terms of the Creative Commons Attribution License, which permits use, distribution and reproduction in any medium, provided the original work is properly cited.

© 2021 The Authors. *Journal of Applied Polymer Science* published by Wiley Periodicals LLC.

Thermoplastic composites reinforced with cellulosic fibers from thermomechanical pulp (TMP) or tissue can be processed using conventional pilot-scale equipment, but the outcome regarding the mechanical properties varies, probably due to aggregation of the fibers.^{9,10} Smaller elements, with better mechanical properties and a theoretically higher reinforcing efficiency, such as CNC or cellulose nanofibrils (CNF), have been reported to be even more prone to form aggregates if precautions are not taken during the melt processing.^{6,11,12} The best method for producing well-dispersed nano-reinforced composites is solvent casting, but this is not a sustainable processing method due to the often-needed toxic organic solvents and difficulties in scaling up. In order to make sustainable cellulose nanocomposites interesting on a commercial level, large-scale processing using conventional melt processing techniques must be developed.⁶

Herrera et al.¹³ showed that liquid-assisted extrusion could improve the dispersion and mechanical properties when cellulose nanofibers and chitin nanocrystals were mixed into a polylactic acid matrix, and it has been suggested that the presence of water could reduce the risk of discoloration and degradation on prolonged exposure to elevated temperatures during melt processing.^{14,15} In view of the reported positive results of water-assisted melt mixing, it has here been decided to explore matrices with different melting temperatures and different surface chemistries, to evaluate the response to water-assisted processing of cellulose-containing composites with regard to dispersion and mechanical behavior. Two thermoplastic matrices have been used for this purpose. Poly(ethylene-co-acrylic acid) (EAA) is a copolymer commonly used in the packaging industry, containing acrylic acid groups, providing good adhesion with a hydrophilic reinforcement.^{10,16–18} As biodegradable alternative to EAA, poly(ϵ -caprolactone) (PCL) was selected considering its biodegradability, high ductility, and toughness, but with a relatively more hydrophobic surface than the EAA.¹⁹ Both matrices have relatively low melting points thus enabling more effective water-assisted extrusion and the possibility of low processing temperatures, which are beneficial to prevent cellulose degradation. The use of cellulose as a reinforcement for both EAA7 and PCL increases their renewable content and can improve their mechanical properties. The pilot-scale processing provides an indication of the feasibility of producing these sustainable composites industrially. In this context, it is also important to assess the possible advantages and disadvantages of using CNC instead of TMP as the reinforcing phase. Nano-sized reinforcements are expected to enhance the mechanical properties of composites, however, further processing steps for the manufacture of CNC may be necessary, and their limited availability and higher cost should also be considered.

In the present work, composite materials with an EAA7 or PCL matrix, reinforced with 10 wt% TMP or CNC, have been produced in pilot-scale industrial facilities in batches of 25 kg. The effects of laboratory-scale and pilot-scale processing conditions on the morphology and mechanical properties of the composites have been evaluated, and the dry and water-assisted processing of different composites have been compared. The compounded batches were injection molded into plaques and evaluated in terms of mechanical, thermal, and rheological properties. An industrially relevant application was also explored, in this case the manufacture of caps for beverage cartons. The compounding step was performed in pilot-scale facilities at Polykemi (Ystad, Sweden) and the subsequent injection molding was carried out at Tetra Pak (Lund, Sweden).

2 | EXPERIMENTAL

2.1 | Materials

Sulfuric-acid-hydrolyzed CNC in the form of a never-dried dispersion, 6 wt% dry content, and as a spray-dried water-dispersible powder were purchased from CelluForce, Canada. The previously characterized CNC have an average length of 301 ± 110 nm and a diameter of 6 ± 3 nm.¹² The CNC powder was dispersed in the never-dried dispersion to a dry content of 8.1 wt% by weight using an IKA T25 digital Ultra Turrax at a speed of 12,000 rpm for 10 min. Fiber-reinforced composites were obtained with a TMP produced from Norwegian spruce, kindly supplied by Stora Enso, Sweden. The TMP had a moisture content of 5.3 wt% and a composition of approximately 47% cellulose, 23% hemicellulose, and 28% lignin (2% nondetected).^{20–22}

Two composites were produced with; a poly(ethylene-acrylic acid) copolymer containing 7% acrylic acid (EAA7), Primacor 3540 from Dow Chemical Company, Sweden and a PCL, Capa 6500, from Ingevity, UK. The EAA7 had a number average molecular weight (M_n) of $16,100 \text{ g mol}^{-1}$, a density of 0.932 g cm^{-3} , a melting point of 88°C and a melt flow rate of 8 g/10 min (ISO 1133) while the PCL had a M_n of $50,000 \text{ g mol}^{-1}$, a melting point of 60°C and a melt flow rate of 7.9–5.9 g/10 min at $190^\circ\text{C}/2.16 \text{ kg}$, according to the suppliers.

2.2 | Production of composites

2.2.1 | Extrusion

CNC- and TMP-reinforced pellets were prepared by a two-step procedure, the first step being a water-assisted mixing for the CNC-based samples, or a dry-mixing for

the TMP-based samples, in a twin-screw extruder (TSE) followed by a homogenizing extrusion (compounding). All the materials were compounded twice in the TSE and pelletized after each extrusion cycle, the aim being to obtain a final cellulose content of 10 wt% in the composites. The compounding was performed using both a laboratory-scale and a pilot-scale equipment, but the water-assisted mixing was mainly carried out using the laboratory-scale equipment. For the laboratory-scale processing, a Werner & Pfleiderer ZSK 30 M9/2 (Stuttgart, Germany) co-rotating TSE having a screw diameter of 30 mm and a screw length of 971 mm was used, and for the pilot-scale production, a Coperion ZSK 26 (Stuttgart, Germany) extruder having a screw diameter of 26 mm and a screw length of 1144 mm was used at Polykemi, Ystad, Sweden.

In the TSE, three different screw configurations were used; a mixing screw (MS), a compounding screw used on a laboratory-scale (CS) and a compounding screw used on a pilot-scale (SPK), as shown in Figure 1 and Table 1. The MS screw configuration was chosen in order to pump and mix the CNC suspension as described by Forsgren et al.,²³ whereas the CS screw, which had two additional kneading elements, was employed to improve the dispersive and distributive mixing during the melt processing on the laboratory-scale. The SPK screw (Figure 1c) was configured to correspond to the description provided by Polykemi. Table 1 shows the residence time in the different screw designs at their respective screw speeds. The longer residence time with the MS screw configuration was due mainly to the presence of large amounts of water coupled to the high backflow of the dispersion.

In the case of the CNC-containing EAA7 and PCL samples, the water-assisted mixing was carried out in the laboratory-scale TSE using either the MS or the SPK screw configuration at 50 rpm (Figure 1, Table 1). The procedure for wet mixing was similar to that described by Forsgren et al.²³ where a dispersion, containing 8.1 wt% CNC in this case, was added to the hopper of the TSE together with the polymer pellets using a peristaltic pump at a feed rate of 23 g min^{-1} (1.9 g dry CNC/min). The feed rates of the EAA7 or PCL was adjusted in order to obtain composites containing 10 wt% of CNC.

In the case of the dry-mixed TMP-based samples, the CS screw configuration was used (Figure 1b, Table 1) at 50 rpm to prepare the laboratory-scale samples, but the SPK screw configuration at screw speeds of 600 and 300 rpm for the EAA7 and PCL samples, respectively, was used for the pilot-scale samples.

The compounding step to homogenize the samples was carried out using the CS screw at a screw speed of 70 rpm for all the laboratory-scale samples. In the pilot-scale

compounding, the second extrusion was performed under the same conditions as the first pilot-scale extrusion.

Different temperature profiles were used for the different matrices and steps in order to ensure a consistent throughput. For the water-assisted mixing of the EAA7-CNC-based samples, the temperature from the hopper to the die was 80–90–130–130–120–120°C, but for the PCL-CNC-based samples it was 40–70–110–120–120–110°C. The second extrusion, the compounding step in the laboratory-scale TSE for the EAA7-based samples, had a temperature profile of 120–140–200–200–170–170°C, whereas the PCL samples were subjected to the same temperature profile as that of the water-assisted mixing. On the pilot-scale, the EAA7-based samples were compounded at a temperature of 140°C over all the 10 heating zones, whereas the PCL-based samples were compounded at 85°C. The residence time was taken as the time until the first trace of aggregates or color change appeared in the melt at the die exit.

2.2.2 | Injection molding

The compounded pellets were dried for 48 h at 65°C and 45°C respectively for the EAA7 and PCL samples, before the final shaping of the compounds into square plates with dimensions of $64 \times 64 \times 1.5 \text{ mm}^3$, using an injection molding machine of the Arburg Allrounder 221 M-250-55 type (Austria). The sprue from the cylinder nozzle to the cavity expanded from a diameter of 4 mm to a diameter of 7 mm along the sprue length of 54 mm, followed by an 18 mm long runner with a cross section of 40 mm^2 and a rectangular cavity gate having a $8 \times 1.5 \text{ mm}^2$ cross section and a land length of 1 mm. The general processing parameters during the injection molding of the different materials are listed in Table 2. The circumferential screw speed was set to 20 m min^{-1} and a backpressure of 1.5 MPa was applied in the plasticization. The injection molding cycle time was 45 s for the EAA7-based and 85 s for the PCL-based materials, including 10 s holding time for both materials but 30 s cooling time for the EAA7 and 70 s cooling for the PCL. The first 25 samples were discarded before the injection molding process was considered stable.

Beverage container caps were injection molded using a Boy 12A at Tetra Pak, Lund, Sweden using the materials compounded on a pilot-scale. The processing parameters during the pilot-scale injection molding are shown in Table 2. A back pressure of 90 bar was applied and the circumferential speed was set to 225 mm s^{-1} . The injection molding cycle time was 64–67 s for the EAA7-based samples and 32 s for the PCL-based materials, including 2 s holding time for both materials.

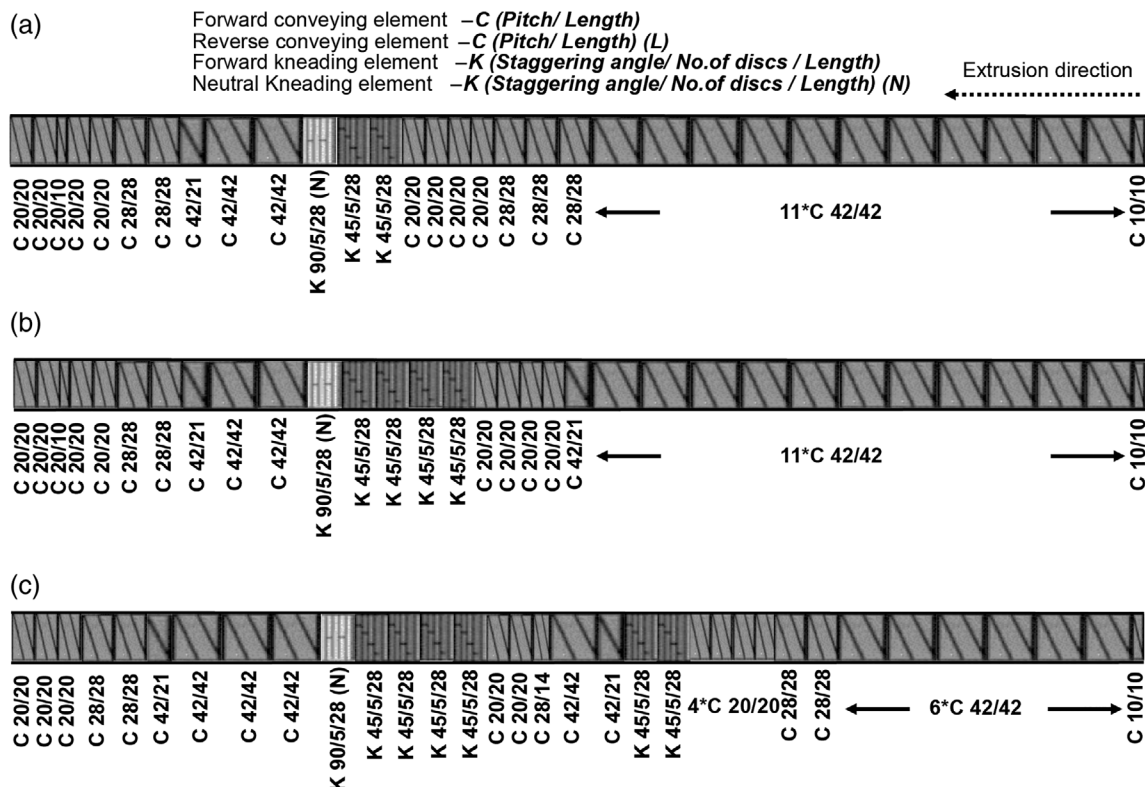


FIGURE 1 The three different screw configurations; (a) The mixing screw (MS), (b) The compounding screw (CS) used on a laboratory scale, (c) The screw type (SPK) used on a pilot scale

TABLE 1 Screw configuration, screw speed, residence time (RT), and throughput at the extrusion die for the various composites

| Sample | Process type | Screw configuration | Screw speed (rpm) | RT (min) | Throughput (kg h ⁻¹) |
|--------------|--------------|---------------------|-------------------|----------|----------------------------------|
| EAA7-CNC-CS | Mixing | MS ^a | 50 | 7.5 | 1 |
| | Compounding | CS | 70 | 2.5 | 3 |
| EAA7-CNC-SPK | Mixing | MS ^a | 50 | 7.5 | 1 |
| | Compounding | SPK | 600 | <1 | 40 |
| PCL-CNC-CS | Mixing | MS ^a | 50 | 7.5 | 1 |
| | Compounding | CS | 70 | 3 | 3 |
| PCL-CNC-SPK | Mixing | SPK ^a | 50 | 7.5 | 1 |
| | Compounding | SPK | 300 | ~1 | 20 |
| EAA7-TMP-CS | Mixing | CS | 50 | 4 | 1 |
| | Compounding | CS | 70 | 1.5 | 3 |
| EAA7-TMP-SPK | Mixing | SPK | 600 | <1 | 40 |
| | Compounding | SPK | 600 | ~1 | 40 |
| PCL-TMP-CS | Mixing | CS | 50 | 3 | 1 |
| | Compounding | CS | 70 | 2 | 3 |
| PCL-TMP-SPK | Mixing | SPK | 300 | <1 | 20 |
| | Compounding | SPK | 300 | ~1 | 20 |

^aWater-assisted mixing.

Note: The gray background indicates pilot-scale and the white background laboratory-scale equipment.

TABLE 2 Processing parameters during the injection molding of square test plates in the laboratory-scale and pilot-scale processing of beverage container caps

| | Sample | Injection speed ($\text{cm}^3 \text{s}^{-1}$) | Injection pressure (bar) | Holding pressure (bar) | Cycle time (s) | Temperature profile from hopper to nozzle ($^{\circ}\text{C}$) |
|-----------------------------|--------------------------|---|--------------------------|------------------------|----------------|--|
| Laboratory-scale processing | All EAA7-based materials | 50/20 | 750 | 800 | 45 | 110–150–150–170–170 |
| | All PCL-based materials | 55/35 | 700 | 750 | 85 | 40–70–110–110–120 |
| Pilot-scale processing | EAA7-CNC-SPK | 16/12 | 1400/1200 | 800 | 64 | 110–150–150–170–170 |
| | EAA7-TMP-SPK | 18/15 | 1900/1700 | 800 | 67 | 110–150–150–170–170 |
| | PCL-CNC-SPK | 10/10 | 1600/1200 | 800 | 32 | 60–75–110–110–120 |
| | PCL-TMP-SPK | 10/10 | 1600/1200 | 800 | 32 | 60–75–110–110–120 |

2.3 | Characterization methods

2.3.1 | Soxhlet extraction

The insoluble TMP and CNC were separated from the soluble PCL fraction from 5 g of PCL-based composites by Soxhlet extraction, the extraction being carried out overnight in glass fiber thimbles (Whatman) using 500 ml of dichloromethane (VWR, 99.5 + % purity) in each Soxhlet extractor.

2.3.2 | Morphology

The morphology of the Soxhlet-extracted CNC was examined, and the cross section of cryo-fractured composites assessed by scanning electron microscopy (SEM), using a Philips XL30 environmental scanning electron microscope (ESEM). The samples were sputtered for 60 s at 10 mA to obtain a 8–10 nm thick coating of gold.

2.3.3 | Fiber analysis

The average fiber length and width were assessed, based on data for approximately 30,000 fibers, according to the Tappi standard T271, using a Kajaani FS300 fiber analyzer (Metso Automation, Finland).

2.3.4 | Thermal gravimetric analysis

Thermal gravimetric analysis (TGA) was used to assess the thermal stability of the materials using a TGA/differential scanning calorimetry (DSC) 3 + Star system (Mettler Toledo, Switzerland). A 3–5 mg sample

was heated at $10^{\circ}\text{C min}^{-1}$ from 25 to 500°C under a nitrogen flow rate of 50 ml min^{-1} .

2.3.5 | Differential scanning calorimetry

The thermal transitions and fusion enthalpies of the materials were assessed using a Mettler Toledo DSC2 calorimeter equipped with a HSS7 sensor and a TC-125MT intercooler. The endotherms were recorded at the first temperature increase from 25 to 160°C at a scan rate of $10^{\circ}\text{C min}^{-1}$ with a nitrogen flow of 50 ml min^{-1} . The degree of crystallinity (X_c) was evaluated according to Equation 1:

$$X_c = \frac{\Delta H_c}{w_M \Delta H_o}, \quad (1)$$

where ΔH_c is the specific heat of fusion of the composite, w_M the weight fraction of the polymer matrix and ΔH_o the specific heat of fusion for a 100% crystalline matrix (277.1 J g^{-1} for EAA7 and 135.6 J g^{-1} for PCL).^{24,25} The melting point (T_m) of the polymer matrix was taken as the peak value of the DSC endotherms and triplicates of each sample were measured.

2.3.6 | Dynamic-mechanical analysis

A Rheometrics RSA II was used to measure the dynamic-mechanical properties of the materials at 23°C . Specimens were cut from the midsection of the molded plaques, the length being in the direction of injection of the plaques, and kept at $23 \pm 2^{\circ}\text{C}$ and $53 \pm 2\%$ r.h. for 48 h prior to the measurement. The specimens were pre-strained to about 0.13% (in tension), which was kept constant during the measurements, and a sinusoidal deformation was superimposed.

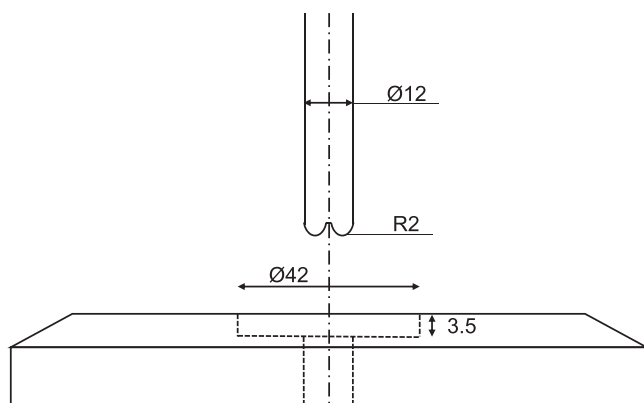


FIGURE 2 Schematic drawing of the fixture used to assess the deformation resistance of the caps in compression. Measurements in mm

The mechanical loss factor ($\tan \delta$) was used as a measure of the relative strength of the interphase region between the matrix and the reinforcement.¹⁷

2.3.7 | Rheological properties

Small-amplitude oscillatory shear (SAOS) tests and steady shear viscosity measurements were carried out on the melts using an Anton Paar MCR 702 rheometer (Graz, Austria) with parallel plate geometry (15 mm plate diameter). Disk-shaped samples were cut from the injection molded plates and kept at $23 \pm 2^\circ\text{C}$ and $53 \pm 2\%$ r.h. for 48 h prior to the measurements with a plate gap of 1 mm and a shear rate range of $0.01\text{--}100\text{ s}^{-1}$.

The rheological properties of the EAA7 and PCL composites were determined at 170°C and 120°C , respectively, after verification of their stability over 50 min, any thermal degradation during the rheological measurements being assumed to be negligible. In the SAOS experiments, the linear viscoelastic region was first assessed using a strain sweep from 1% to 100% at a constant angular frequency of 1 s^{-1} , followed by angular frequency sweeps in the range of $0.08\text{--}200\text{ s}^{-1}$ at strain amplitudes of 0.04%–0.7%. The experiments were repeated twice using duplicate specimens.

2.3.8 | Mechanical properties

A Zwick/Z2.5 tensile tester equipped with a 2 kN load cell was used to measure the tensile properties of the injection molded materials. Tensile test bars, with a gauge length of 40 mm and a thickness of about 1.5 mm, were cut from the midsection of the injection molded plaques, along the direction of injection, and tested after

conditioning at $23 \pm 2^\circ\text{C}$ and $53 \pm 2\%$ r.h. for 48 h. The Young's modulus, tensile strength at yield, ultimate tensile strength, and elongation at break were measured at 25°C at a strain rate of $2.5 \times 10^{-3}\text{ s}^{-1}$. The reported values are the average values of five or six independent measurements.

The same tensile tester was used to assess the deformation resistance of the injection-molded beverage caps. The caps were center-point fixed in an aluminum fixture with a depression of 3.5 mm and with a diameter corresponding to that of the cap. A steel piston with rounded tip and a hole in the center to avoid contact with the gate mark on the cap was used to compress the samples at a piston speed of 13 mm min^{-1} , corresponding to one cap height per minute, as shown schematically in Figure 2. The structural stiffness and maximum force of the caps during compression were measured at 25°C after conditioning the caps at $23 \pm 2^\circ\text{C}$ and $53 \pm 2\%$ relative humidity for 48 h. The reported values are the average values of five independent measurements.

3 | RESULTS AND DISCUSSION

Batches of 25 kg of CNC- and TMP-reinforced thermoplastic pellets were successfully prepared using a combination of wet mixing and compounding with TSE on a laboratory and a pilot scale. The TSE and injection-molding parameters were adapted, as shown in Figure 1, Tables 1 and 2. Square plates were successfully obtained by injection molding on a laboratory scale, and beverage container caps were successfully injection molded on a pilot scale.

3.1 | Visual appearance and morphology

Figure 3 shows the difference in visual appearance of the injection-molded EAA7-CNC and EAA7-TMP plaques compounded on a pilot scale (SPK) and on a laboratory-scale (CS). Despite using water-assisted extrusion, the CNC-reinforced samples compounded using the CS screw configuration appeared to contain larger aggregates and were darker in color, perhaps as a consequence of the longer residence time and lower screw speeds used in the CS than in the SPK system. Similar sort of behavior has been observed in cellulose-based systems where an increased amount of moisture exhibited larger aggregates owing to a combination of low shear and Leidenfrost effects.⁹ Similar differences were observed between the TMP-reinforced samples. When cellulosic materials are processed for long periods of time, at a high-temperature degradation can occur, and this might result in discoloration of the composites.²⁶ The presence of larger agglomerates in CS

FIGURE 3 Photographs of injection molded samples of EAA7 reinforced with 10% CNC (a, b) and TMP (c, d) Compounded on a laboratory scale (CS) and on a pilot scale (SPK). CNC, cellulose nanocrystals; TMP, thermomechanical pulp [Color figure can be viewed at wileyonlinelibrary.com]

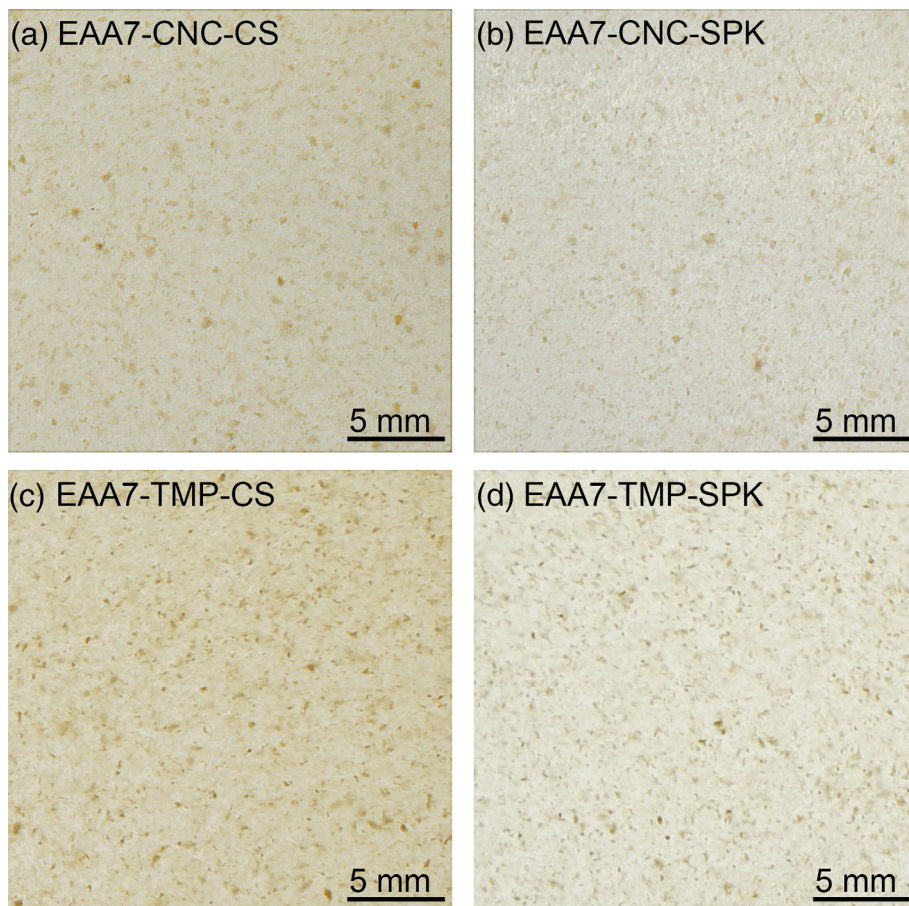
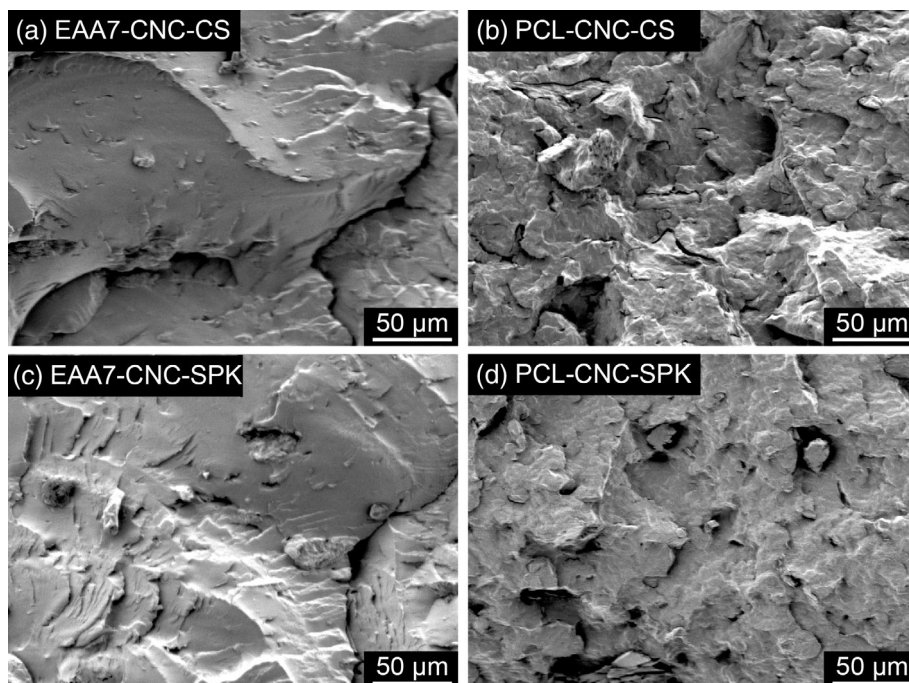


FIGURE 4 Scanning electron microscopy (SEM) images of cryo-fractured surfaces of injection-molded 10% CNC-reinforced (a, c) EAA7 and (b, d) PCL composites compounded on (a, b) a laboratory scale and (c, d) a pilot scale. CNC, cellulose nanocrystals; PCL, poly(caprolactone)



material than in the SPK equivalent indicates a poorer dispersion of the reinforcement by the CS configuration, probably due to lower shear forces at the lower screw speeds.

SEM-micrographs of cryo-fractured surfaces of the injection-molded EAA7 and PCL samples reinforced with 10% CNC and TMP, compounded on the laboratory- or pilot-scale are shown in Figures 4 and 5, respectively. The

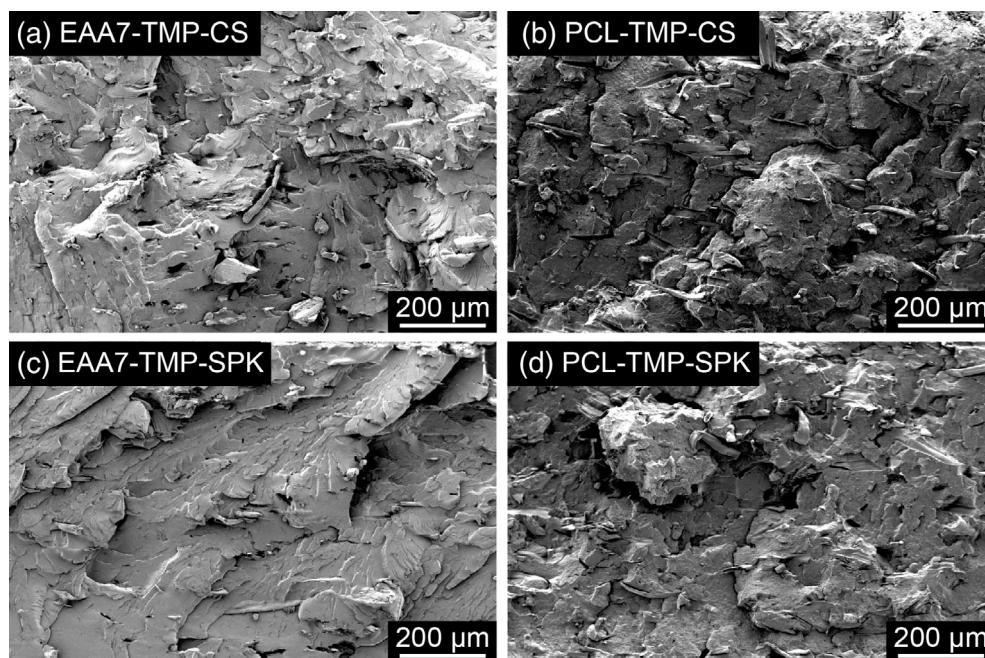


FIGURE 5 Cryo-fractured surfaces of injection molded 10% TMP reinforced (a, c) EAA7 and (b, d) PCL composites compounded on (a, b) a laboratory-scale and (c, d) a pilot-scale. CNC, cellulose nanocrystals; PCL, poly(caprolactone); TMP, thermomechanical pulp

micrographs in Figure 4 showed that there is a clear difference between the cryo-fractured surfaces of the PCL-CNC and the EAA7-CNC samples with regard to voids and roughness, regardless of the method of compounding. The CNC aggregates seem to be embedded in the EAA7 with a good adhesion and no pull-out, Figure 4a, c, whereas they appear to be dislodged in the PCL-based samples. The presence of polar acrylic acid groups on the EAA7 chains make the polymer relatively more hydrophilic and thus improve the EAA7-CNC compatibility.^{10,18} The poorer adhesion between PCL and CNC is also reflected in the higher surface roughness of the PCL-based composites.

To investigate the effect of the processing conditions on the final composite properties, the PCL was Soxhlet extracted from the PCL-CNC-based samples, selected because PCL is more soluble than EAA7 in organic solvents like dichloromethane. Pristine CNC has a rod-like structure,¹² but the CNC recovered from the composite (Figure 6) was aggregated and had a low aspect ratio. Some caution must however be observed when interpreting these results, since the aggregates could be a consequence of the Soxhlet extraction and subsequent drying of the recovered CNC.

The fracture surfaces of the TMP-reinforced samples, shown in Figure 5, revealed that the EAA7-based samples had a more compact surface with only a few fibers being exposed in the fractured surface, confirming that there was good adhesion between EAA7 and the TMP. In contrast, the fractured surface of the PCL samples revealed exposed fibers and many voids, indicating the pull-out and debonding typical of poor interfacial adhesion.

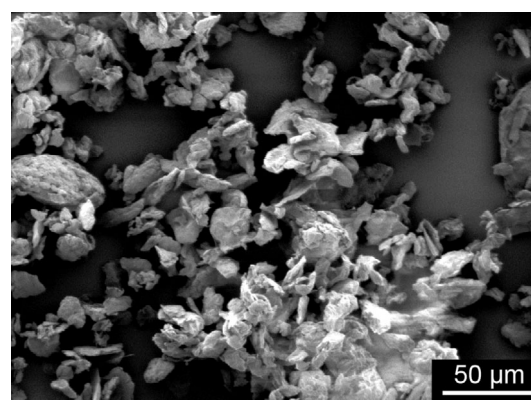


FIGURE 6 Scanning electron microscopy (SEM) micrograph of CNC recovered from the PCL-based composites by Soxhlet extraction from dichloromethane. CNC, cellulose nanocrystals; PCL, poly(caprolactone)

TABLE 3 Analysis of as received TMP fibers and of TMP fibers extracted from compounded PCL composites

| Sample | Length (mm) | Width [μm] | Aspect ratio |
|-------------|-------------|------------|--------------|
| TMP | 2.8 | 36 | 78 |
| PCL-TMP-CS | 0.68 | 27 | 25 |
| PCL-TMP-SPK | 0.5 | 25 | 20 |

The differences between the samples processed under different conditions were not sufficient in the SEM micrographs (Figures 4 and 5), to enable obvious conclusions to be drawn, although the higher shear forces in the pilot-scale process were expected to break the aggregates.

After processing there was a significant reduction in fiber dimensions, somewhat greater after the pilot-scale than after the laboratory-scale compounding, see Table 3. The pilot-scale compounding reduced the average length and width of the fiber from 2.8 mm and 36 μm , to 0.5 mm and 25 μm , respectively, whereas the laboratory-scale compounding gave a reduction to 0.68 mm and 27 μm , respectively.

3.2 | Thermal properties

Table 4 summarizes the thermal properties of the EAA7 and PCL samples reinforced with CNC and TMP after compounding under different processing conditions. Neither the crystallinity nor the melting point was significantly affected by the addition of CNC or TMP, regardless of the processing conditions. The thermo-gravimetric analysis indicated that the presence of the reinforcement reduced the thermal stability of the matrix (second temperature indicated), although neither the process design nor the process parameters seemed to affect the onset of degradation (T_{onset}). The CNC composites had a lower thermal stability than the TMP composites, which reflects the higher thermal stability of pristine TMP than of CNC, probably because of its higher lignin content.^{27–29} The PCL-TMP composites exhibited only one degradation peak at an average onset temperature of 370°C, related to PCL degradation, and it appears that shielding of the TMP by the PCL delays the TMP degradation. Two onset-of-degradation temperatures were registered for the other composites, where the first is related to the degradation of the cellulosic component. In case of the CNC-containing specimens, this temperature was in the 265–269°C range, which is about 30°C higher than that of the pristine CNC. For the EAA7-TMP composites, the initial degradation was observed at 300°C, which is about 20°C higher than that of the pristine TMP. Both these results thus indicate that the thermal stability of the cellulose was increased when it was embedded in the polymer matrices. However, the onset temperatures of the matrix reduced for all the composites, and this has been previously observed in cellulose-based composites where the presence of cellulosic reinforcements that degrade at relatively lower temperatures, could result in creation of reactive compounds, which affect the thermal stability of the matrix.^{30,31}

3.3 | Dynamic mechanical analysis

Strain sweep measurements of the dynamical mechanical loss factor were made study the interphase properties of the different composites. Figure 7 shows the mechanical

loss factor ($\tan \delta$) as a function of the applied strain amplitude for the CNC- and TMP-reinforced composites, compounded under different conditions. In the case of the EAA7 samples, Figure 7a, the loss factor was independent of the strain amplitude, indicating a stable interphase region and good adhesion between the EAA7 and cellulosic materials, not affected by the processing conditions.

In the case of the PCL-based samples, Figure 7b, larger changes were however seen. The slope of the loss factor with increasing strain amplitude increased markedly for both the CNC-SPK and the TMP-SPK samples, which may indicate a partial disruption of the interphase as the deformation increased, resulting in mechanical losses. The TMP-CS specimen exhibited a minor $\tan \delta$ plateau at lower strain amplitudes, followed by an increasing $\tan \delta$ with increasing strain amplitude, which may indicate that the interphase failed at a critical strain. In the case of the CNC-CS samples, $\tan \delta$ showed only a weak dependence on the strain amplitude, suggesting a more stable interphase region. Wet mixing using the milder screw configuration (MS) and compounding with the CS screw configuration with lower screw speeds, higher temperatures, and longer residence times, thus appeared to increase the mechanical stability of the interphase in the PCL-CNC composites.

3.4 | Melt rheology

3.4.1 | Small amplitude oscillatory shear

The oscillatory strain sweeps at 170°C shown in Figure 8a for the EAA7-based composites prepared on a laboratory scale (EAA7-CNC-CS and EAA7-TMP-CS) revealed a storage modulus (G') higher than that of the matrix, the G' value of the TMP-CS being the largest. The G' value of the CNC-SPK was similar to that of the matrix at low-shear strain values, but the modulus then increased markedly with increasing shear strain up to a maximum value, after which it decreased. A similar maximum was observed for the CNC-CS and TMP-CS samples, suggesting the presence of a cellulosic network, which resists deformation as, observed in CNC-based and other polymeric systems containing a structural network.^{23,32,33} The existence of a structural network does not however imply that there is physical contact between the cellulosic particles but merely indicates an overlapping of regions in the polymer matrix that are affected or reinforced by the cellulosic entities. The affinity between the cellulosic elements and the polymer matrix clearly plays a role. For all the samples exhibiting a maximum in G' , the loss modulus (G'') was greater than the

| Sample | Crystallinity (%) | Melting point (°C) | T_{onset} (°C) |
|--------------|-------------------|--------------------|-------------------------|
| CNC | — | — | 236 ± 2 |
| TMP | — | — | 284 ± 4 |
| EAA7 | 16 ± 1 | 98 ± 2 | 430 ± 10 |
| EAA7-CNC-CS | 16 ± 1 | 99 ± 1 | $265 \pm 5; 415 \pm 5$ |
| EAA7-CNC-SPK | 15 ± 1 | 99 ± 1 | $268 \pm 3; 419 \pm 5$ |
| EAA7-TMP-CS | 16 ± 2 | 99 ± 1 | $300 \pm 5; 415 \pm 2$ |
| EAA7-TMP-SPK | 15 ± 1 | 99 ± 1 | $300 \pm 2; 417 \pm 2$ |
| PCL | 51 ± 1 | 60 ± 2 | 375 ± 6 |
| PCL-CNC-CS | 51 ± 1 | 60 ± 2 | $269 \pm 2; 365 \pm 3$ |
| PCL-CNC-SPK | 54 ± 2 | 59 ± 3 | $268 \pm 3; 364 \pm 2$ |
| PCL-TMP-CS | 51 ± 2 | 61 ± 1 | 370 ± 7 |
| PCL-TMP-SPK | 50 ± 1 | 62 ± 2 | 370 ± 5 |

TABLE 4 The degree of crystallinity, melting point assessed by DSC analysis and onset temperature for the onset of thermal degradation evaluated by TGA for the CNC and TMP, the polymer matrices and the composites

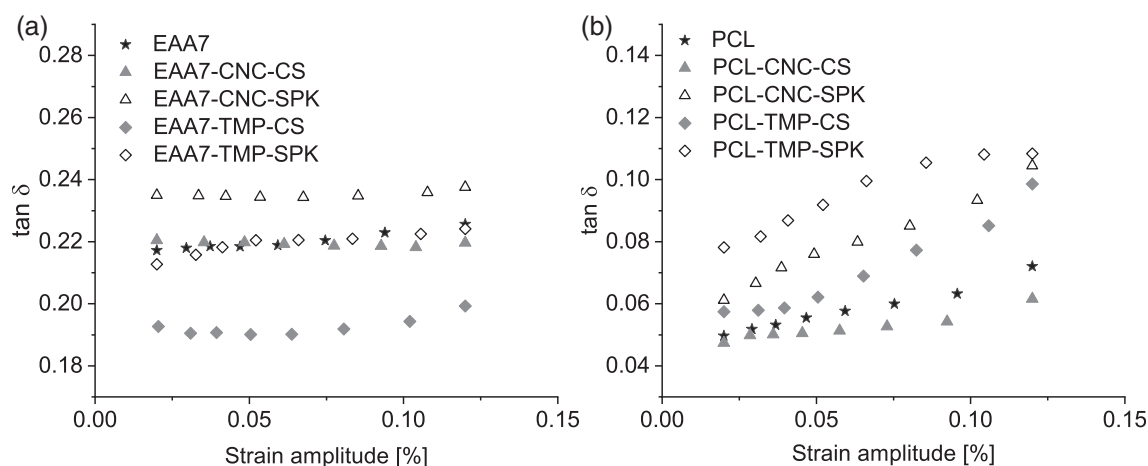


FIGURE 7 Mechanical loss factor ($\tan \delta$) as a function of applied strain amplitude for the injection-molded (a) EAA7-based and (b) PCL-based composites containing 10 wt% CNC and TMP after compounding using CS and SPK screw configurations. CNC, cellulose nanocrystals; PCL, poly(caprolactone); TMP, thermomechanical pulp

storage modulus up to a critical shear strain (cross-over points at $G' = G''$) after which $G' > G''$ for the samples, corresponding to a solid-like transition in the rheological behavior. These composites thus displayed a strong nonlinear viscoelastic behavior. The only sample that exhibited a constant G' over the entire range of the applied shear strain and a $G'' > G'$, was TMP-SPK suggesting a rather poorly developed cellulosic network in this case, which could be because the combination of higher screw speeds and a screw configuration (SPK) induced higher shear forces.

The frequency sweep curves for the EAA7 samples in Figure 8b show that the CNC-CS samples had a higher G' value than the CNC-SPK sample over the examined frequency range. In both cases a weak plateau was observed at low frequencies, more prominently for the CNC-CS, despite $G'' > G'$ throughout the frequency range. The TMP-CS

composite, which was the only material with $G' > G''$ at lower frequencies, also displayed this plateau, as did the TMP-SPK sample, although this was not very prominent. The plateau at lower frequencies suggests the formation of an interconnected structure^{12,34,35} in samples compounded for longer residence times at higher temperatures.

The oscillatory strain sweep for the PCL-based samples at 120°C shown in Figure 9a revealed a G' higher than that of the matrix for both the CNC-containing and TMP-containing samples, the largest increase being at least two orders of magnitude for the TMP samples. Among the CNC-containing samples, which exhibited a constant G' over the entire shear strain amplitude range, the CNC-SPK had a marginally higher G' than the CNC-CS. The TMP-containing samples, Figure 9c, d, with the largest increase in G' among the PCL-based samples, exhibited shorter span of the linear viscoelastic region

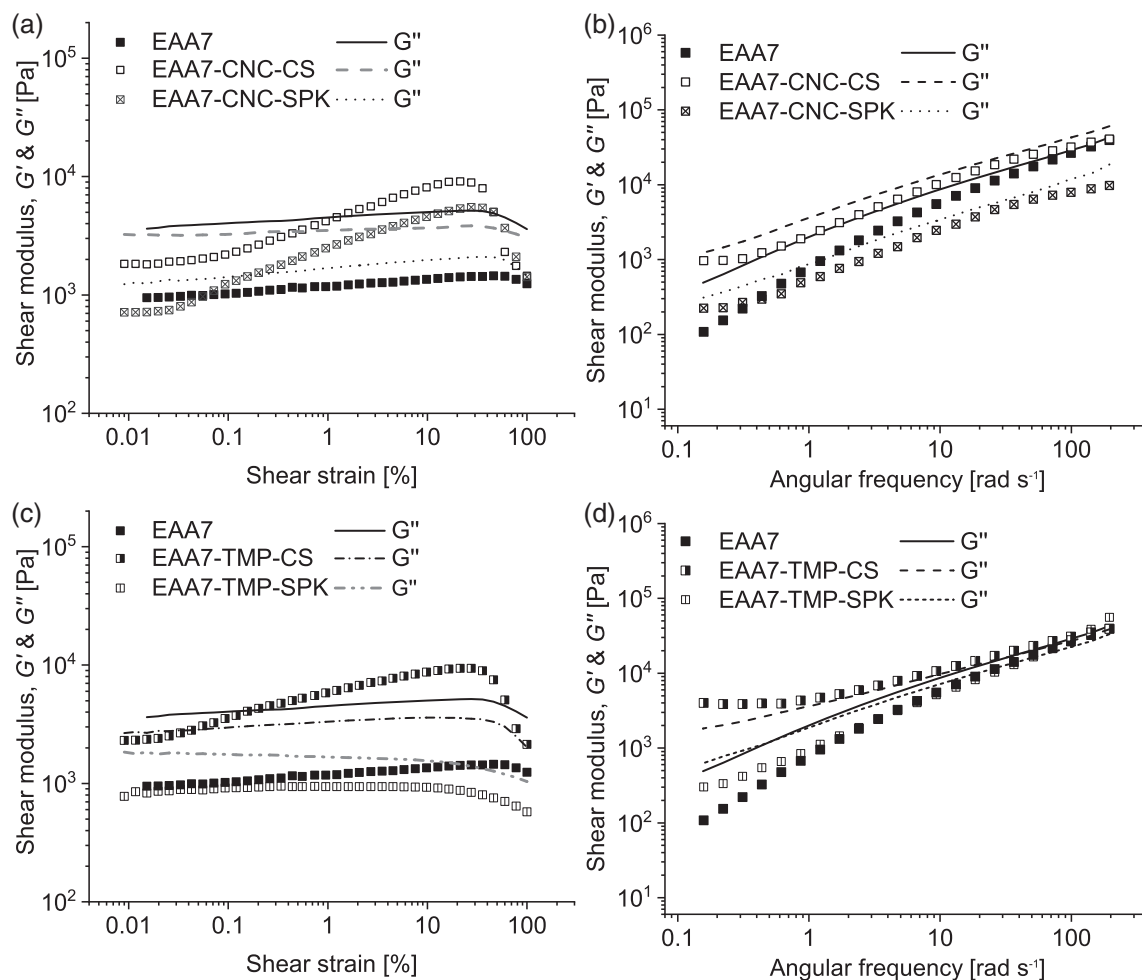


FIGURE 8 The storage and loss moduli (G' , G'') in the melt at 170°C as a function of (a, c) shear strain amplitude and (b, d) angular frequency for the injection-molded EAA7 composites reinforced with 10 wt% (a, b) CNC and (c, d) TMP after being compounded using CS and SPK screw configurations. CNC, cellulose nanocrystals; TMP, thermomechanical pulp

than the CNC-containing samples. For the PCL-based samples, $G'' > G'$ in all the cases.

For the PCL-based samples, the frequency sweeps displayed a more viscous behavior with $G'' > G'$. The CNC-containing samples exhibited a plateau at low frequencies with the CNC-CS having a slightly higher G' . In case of the CNC samples, a plateau was observed at G' values as low as 10–30 Pa. The TMP-containing samples, on the other hand, had a plateau at G' values around 10^3 Pa at low frequencies, with TMP-SPK having a marginally higher G' . These plateaux at lower frequencies can be ascribed to an interconnected structure formation, as previously discussed in the case of EAA7 composites.^{12,34,35}

3.4.2 | Steady shear viscosity

Figure 10 shows the steady shear viscosity of the EAA7 and PCL samples at 170°C and 120°C, respectively,

measured in the shear rate range from 0.01 to 100 s^{-1} . In the case of the EAA7-based samples, the TMP-CS was the only composite showing a viscosity higher than that of the neat matrix. This is consistent with its liquid-to-solid transition behavior observed in the frequency sweep (Figure 8d). All the other composites showed a viscosity lower than that of neat EAA7, probably due to their viscous behavior ($G'' > G'$) revealed by their frequency sweep measurements (Figure 8b, d). This suggests that the network in the TMP-CS sample was stronger than that of the TMP-SPK sample, possibly due to the difference in process conditions. All the composites as well as the neat polymers exhibited a Newtonian viscosity plateau at low shear rates followed by a shear thinning region with increasing shear rate. The EAA7-based composites displayed a shear thinning more pronounced than that of the matrix itself.

In case of the PCL-based samples, only the CNC-SPK composite had a viscosity lower than that of the matrix, whereas the CNC-CS composite showed a slightly higher

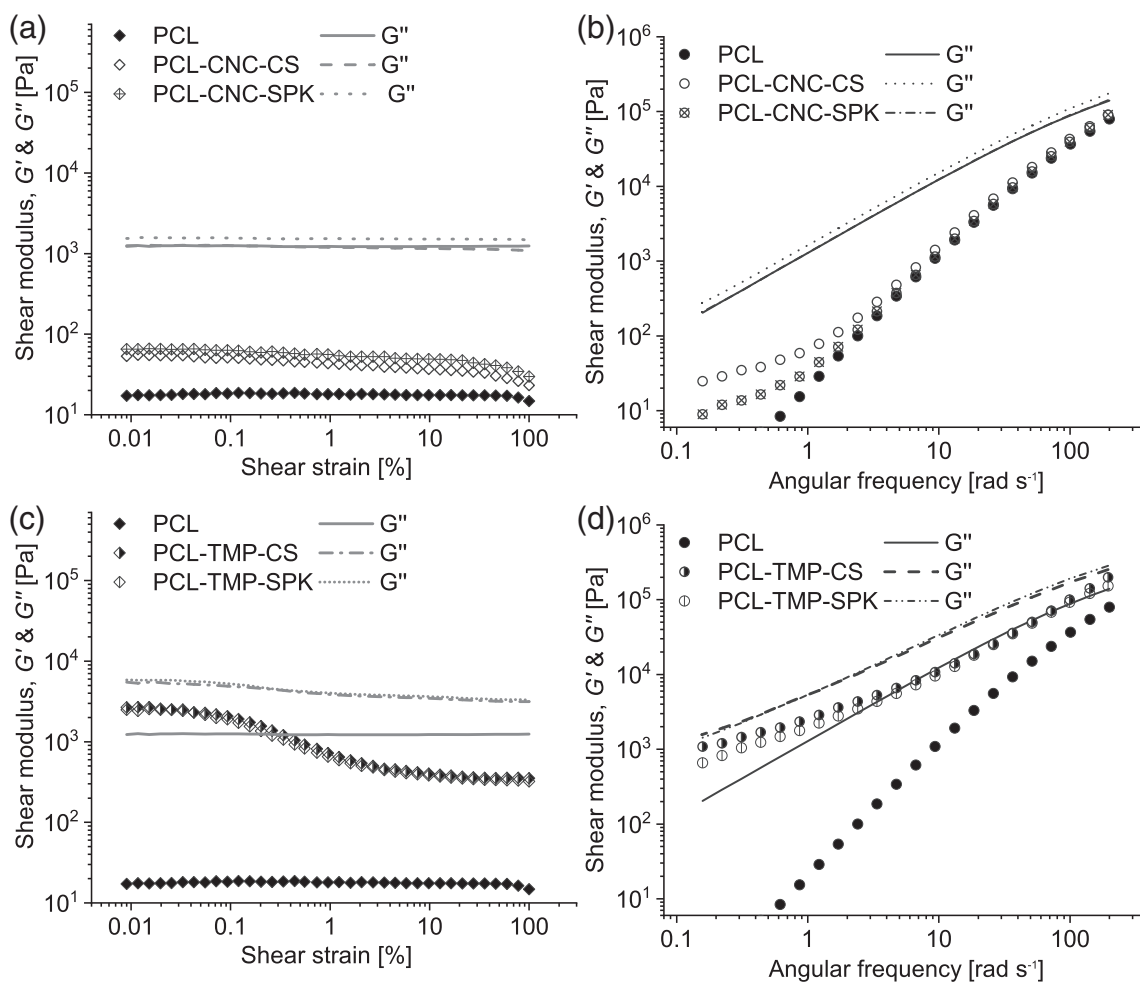


FIGURE 9 The storage and loss moduli (G' , G'') in the melt at 120°C as a function of (a, c) Shear strain amplitude and (b, d) Angular frequency for the injection-molded PCL composites reinforced with 10 wt% (a, b) CNC and (c, d) TMP after being compounded using laboratory-scale (CS) and pilot-scale (SPK) screw configurations. CNC, cellulose nanocrystals; PCL, poly(caprolactone); TMP, thermomechanical pulp

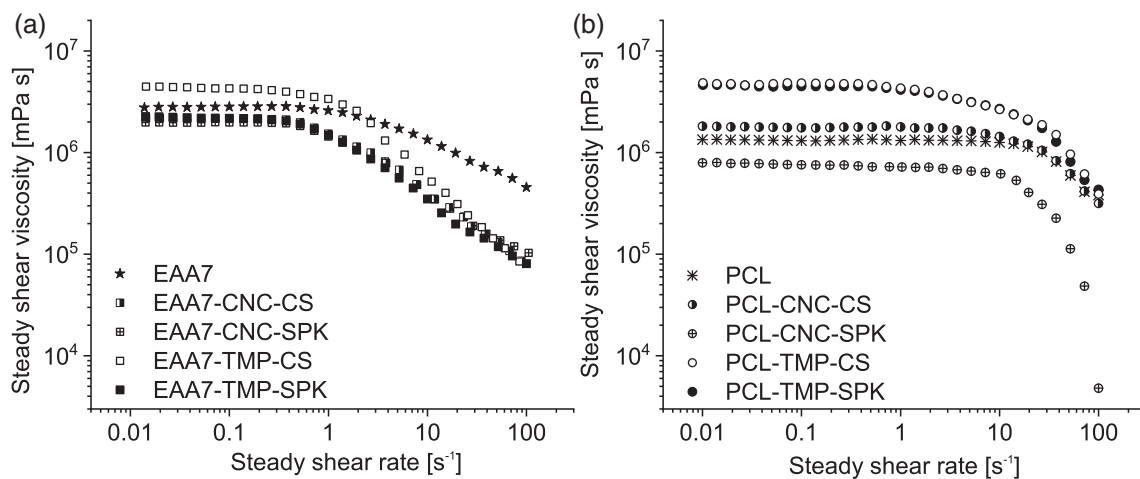


FIGURE 10 The steady shear viscosity as function of shear rate for the injection-molded (a) EAA7 (at 170°C) and (b) PCL (at 120°C) composites reinforced with 10 wt% CNC and TMP after being compounded using CS and SPK screw configurations. CNC, cellulose nanocrystals; PCL, poly(caprolactone); TMP, thermomechanical pulp

value than that of the neat PCL. The PCL composites containing TMP exhibited similar viscosities significantly higher than those of the matrix, regardless of the process conditions.

3.5 | Mechanical properties

The results of the tensile tests are as summarized in Table 5. In the case of the EAA7-based composites, the Young's modulus relative to the matrix was greater by a factor of 1.5 for the CNC-containing samples and by a factor of

2.1 for those containing TMP. This shows the greater reinforcing effect of TMP than of CNC, probably due to higher aspect ratio of the fibers. In the case of the CNC-containing samples, the laboratory-scale (CS) configuration gave the greatest increase in Young's modulus and yield strength from 109 MPa and 5.7 MPa, respectively, to 165 MPa and 7.5 MPa, respectively, whereas the CNC-SPK combination resulted in values of 144 MPa and 6.7 MPa, respectively.

In the case of EAA7 reinforced with TMP, the TMP-CS composite showed a Young's modulus and yield strength of 231 MPa and 11 MPa, respectively, compared with 185 MPa and 8 MPa, respectively, for the TMP-SPK

TABLE 5 Tensile properties of the injection-molded composites

| Sample | Young's modulus (MPa) | Yield stress (MPa) | Ultimate tensile strength (MPa) | Elongation at break (%) |
|--------------|-----------------------|--------------------|---------------------------------|-------------------------|
| EAA7 | 109 ± 2 | 5.7 ± 0.1 | 16.8 ± 0.6 | 91 ± 3 |
| EAA7-CNC-CS | 165 ± 15 | 7.5 ± 0.1 | 16 ± 0.2 | 60 ± 2 |
| EAA7-CNC-SPK | 144 ± 4 | 6.7 ± 0.2 | 15 ± 0.5 | 86 ± 3 |
| EAA7-TMP-CS | 231 ± 3 | 11 ± 0.2 | 15 ± 0.3 | 38 ± 4 |
| EAA7-TMP-SPK | 185 ± 12 | 8 ± 0.3 | 15 ± 0.3 | 59 ± 2 |
| PCL | 414 ± 10 | 16.8 ± 0.1 | 40 ± 0.7 ^a | >810 |
| PCL-CNC-CS | 482 ± 17 | 14 ± 0.3 | 25 ± 0.3 ^a | 540 ± 7 |
| PCL-CNC-SPK | 396 ± 7 | 13 ± 0.2 | 22 ± 3 ^a | 492 ± 61 |
| PCL-TMP-CS | 592 ± 5 | 15 ± 0.3 | 15 ± 0.3 | 307 ± 33 |
| PCL-TMP-SPK | 609 ± 2 | 15 ± 0.3 | 15 ± 0.2 | 291 ± 67 |

^aStrain hardening of the samples.

Note: Each value is the average of 5–6 measurements, with the SD.

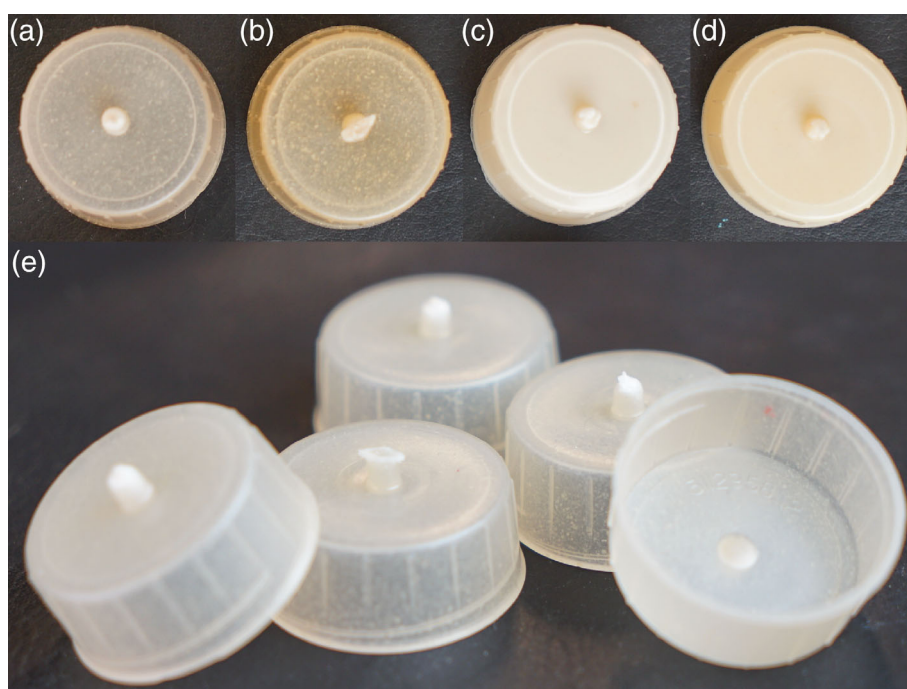


FIGURE 11 Photographs of injection molded beverage containers caps of (a) EAA7-CNC-SPK, (b) EAA7-TMP-SPK, (c) PCL-CNC-SPK, (d) PCL-TMP-SPK, and (e) Several caps of EAA7-CNC-SPK. CNC, cellulose nanocrystals; PCL, poly(caprolactone); TMP, thermomechanical pulp [Color figure can be viewed at wileyonlinelibrary.com]

samples. The milder reinforcing effect of the cellulosic reinforcement in the latter case may be due to a greater shortening of the fibers induced by the higher shear in the pilot-scale process, see Figure 3. The lower values achieved with the SPK screw configuration could be due to the tougher screw design, intended to improve the dispersive and distributive mixing, combined with the higher screw speed, which probably led to greater shear forces and a higher temperature. The elongation at break was quite high for the SPK-produced samples, see Table 5. The lower viscosities recorded for the pilot-scale composites compared to that of the neat EAA7 (Figure 10a) suggest both fiber shortening and polymer degradation.

In the case of the PCL composites, the laboratory-scale processing led to CNC-containing composites with slightly better mechanical properties than those compounded on a pilot scale. The CNC-CS samples had a Young's modulus and yield strength of 482 MPa and 14 MPa, respectively, compared to 396 MPa and 13 MPa, respectively, of the CNC-SPK based samples. The Young's modulus of the CNC-SPK composite was similar to that of the matrix. The yield strength of all the composites was lower than that of the matrix.

The PCL-TMP composites showed no significant differences in tensile properties. This result is supported by the melt rheology data, where data for the laboratory-scale (CS) and pilot-scale (SPK) configurations overlapped.

3.6 | Beverage caps

To investigate a possible application for the composites prepared, beverage caps were successfully injection molded with the pilot-plant equipment at Tetra Pak (Figure 11). The transparency of the EAA7-based samples revealed aggregates of the reinforcing cellulose, whereas the PCL-based samples showed no inhomogeneity, probably due to the higher crystallinity and non-transparency of PCL. All the materials showed a slight yellowing, but the CNC-reinforced caps (Figure 11a, c) showed less discoloration than the TMP-reinforced caps (Figure 11b, d, e). All the caps displayed high fidelity to the mound, fulfilling the main geometrical requirement such as threads visible on the inside of the caps without any indications of irregularities in flow during injection.

The resistance to mechanical deformation of the caps was assessed in terms of structural stiffness and maximum force load at deformation. The results are summarized in Table 6. The ductile character of all the produced caps allowed deformation, but no fractures were registered. The PCL-based caps showed greater structural stiffness than the EAA7-based caps, where the PCL-TMP-SPK exhibited the highest stiffness and the highest

TABLE 6 Structural stiffness and maximum force withstood by caps produced as an example of a potential application of the composites produced in this work

| Sample | Structural stiffness (N mm ⁻¹) | Maximum force (N) |
|----------------|--|-------------------|
| EAA7-CNC-SPK | 17 ± 1 | 105 ± 2 |
| EAA7-TMP-SPK | 17 ± 0.4 | 112 ± 2 |
| PCL-CNC-SPK | 34 ± 2 | 205 ± 5 |
| PCL-TMP-SPK | 41 ± 1 | 228 ± 5 |
| HDPE reference | 46 ± 3 | 316 ± 10 |

maximum force at indentation. High-density polyethylene (HDPE) caps were studied as reference. The HDPE was expected to have a greater structural stiffness than the neat EAA7 and PCL, but the addition of 10 wt% cellulose-based reinforcement into the matrixes was sufficient to raise the PCL to similar values. The feasibility of the melt processing, the fidelity in the shaping to complex geometrical features and good mechanical performance of the caps demonstrate their potential as a sustainable replacement for the polyethylene caps, traditionally used in this application chosen.

4 | CONCLUSION

The feasibility of using water-assisted mixing to manufacture 10 wt% CNC-reinforced beverage caps through traditional melt processing techniques on a pilot scale was shown to be successful. The samples compounded with a pilot-scale TSE, showed smaller cellulose aggregates than samples compounded with a laboratory-scale TSE. Both CNC and TMP recovered after Soxhlet extraction of PCL-based composites had an aspect ratio reduced by the processing. Although the laboratory-scale processing resulted in slightly larger cellulose aggregates, the compounded materials showed a higher melt viscosity and improved tensile properties. The rheological measurements on most of the samples suggest that there is a percolating network in the melt, but the network in the materials compounded in the pilot-scale process had a lower strength. The laboratory-scale compounding led to an overestimation of the overall properties of the samples. EAA7-based composites showed higher relative reinforcement than the PCL-based composites, possibly due to its more hydrophilic character and more stable adhesion to the cellulose. Beverage caps produced with PCL-TMP composites appeared to be a promising alternative to HDPE caps, thanks to the higher stiffness of the neat PCL than that of the EAA7, further improved with cellulose reinforcement.

Conventional cellulose fibers provided matrices with slightly superior mechanical reinforcement than CNC.

ACKNOWLEDGMENTS

The authors thank the Swedish Research Council Formas, Swedish Foundation for Strategic Research and Knut och Alice Wallenbergs Stiftelsen Biokompositforskning for financial support and Chalmers Tekniska Högskola, where the research has been carried out. The authors thank Polykemi and Tetra Pak for collaboration and for the use of pilot-scale equipment. Dr J. A. Bristow is gratefully acknowledged for the linguistic revision of the manuscript.

CONFLICT OF INTEREST

The authors declare no conflict of interest.

ORCID

Abhijit Venkatesh  <https://orcid.org/0000-0001-7365-2921>

Lilian Forsgren  <https://orcid.org/0000-0003-0607-5030>

Angelica Avella  <https://orcid.org/0000-0001-8844-4789>

Fabiola Vilaseca  <https://orcid.org/0000-0001-7752-3158>

Giada Lo Re  <https://orcid.org/0000-0001-8840-1172>

Antal Boldizar  <https://orcid.org/0000-0002-8695-1688>

REFERENCES

- [1] R. Geyer, J. R. Jambeck, K. L. Law, *Sci. Adv.* **2017**, 3, e1700782.
- [2] D. Nabi Saheb, J. P. Jog, *Adv. Polym. Technol.* **1999**, 18, 351.
- [3] A. Dufresne Nanocellulose, *From Nature to High Performance Tailored Materials*, De Gruyter, Berlin/Boston, Germany **2017**.
- [4] T. Saito, S. Kimura, Y. Nishiyama, A. Isogai, *Bio-macromolecules* **2007**, 8, 2485.
- [5] J. Cowie, E. M. M. T. Bilek, T. H. Wegner, J. A. Shatkin, *Tappi J* **2014**, 13, 57.
- [6] K. Oksman, Y. Aitomäki, A. P. Mathew, G. Siqueira, Q. Zhou, S. Butylina, S. Tanpichai, X. Zhou, S. Hooshmand, *Compos. Part A Appl. Sci. Manuf.* **2016**, 83, 2.
- [7] K. Y. Lee, Y. Aitomäki, L. A. Berglund, K. Oksman, A. Bismarck, *Compos. Sci. Technol.* **2014**, 105, 15.
- [8] X. Xu, F. Liu, L. Jiang, J. Y. Zhu, D. Haagensohn, D. P. Wiesenborn, *ACS Appl. Mater. Interfaces* **2013**, 5, 2999.
- [9] M. Hietala, K. Oksman, *Compos. Part A Appl. Sci. Manuf.* **2018**, 109, 538.
- [10] R. Ariño, A. Boldizar, *Polym. Eng. Sci.* **2012**, 52, 1951.
- [11] A. Sato, D. Kabusaki, H. Okumura, T. Nakatani, F. Nakatsubo, H. Yano, *Compos. Part A Appl. Sci. Manuf.* **2016**, 83, 72.
- [12] A. Venkatesh, J. Thunberg, K. Sahlin-Sjövald, M. Rigdahl, A. Boldizar, *Polym. Eng. Sci.* **2020**, 60, 956.
- [13] N. Herrera, A. A. Singh, A. M. Salaberria, J. Labidi, A. P. Mathew, K. Oksman, *Polymer* **2017**, 9, 406.
- [14] J. Karger-Kocsis, Á. Kmetty, L. Lendvai, S. Drakopoulos, T. Bárány, *Materials (Basel)* **2014**, 8, 72.
- [15] T. A. T. Yasim-Anuar, H. Ariffin, M. N. F. Norrahim, M. A. Hassan, Y. Andou, T. Tsukegi, H. Nishida, *Polymer* **2020**, 12, 927.
- [16] A. Venkatesh, J. Thunberg, T. Moberg, M. Klingberg, L. Hammar, A. Peterson, C. Müller, A. Boldizar, *Cellulose* **2018**, 25, 4577.
- [17] L. Forsgren, K. Sahlin-Sjövald, A. Venkatesh, J. Thunberg, R. Kádár, A. Boldizar, G. Westman, M. Rigdahl, *J. Mater. Sci.* **2019**, 54, 3009.
- [18] A. Peterson, A. Y. Mehandzhyski, L. Svenningsson, A. Ziolkowska, R. Kádár, A. Lund, L. Sandblad, L. Evenäs, G. Lo Re, I. Zozoulenko, C. Müller, *Macromolecules* **2021**, 54, 2305.
- [19] G. Lo Re, J. Engström, Q. Wu, E. Malmström, U. W. Gedde, R. T. Olsson, L. Berglund, *ACS Appl. Nano Mater.* **2018**, 1, 2669.
- [20] L. Forsgren, E. C. B. Noyan, A. Vega, N. Yarahmadi, A. Boldizar, *Polym. Degrad. Stab.* **2020**, 181, 109374.
- [21] H. Kangas, M. Kleen, *Nord. Pulp Paer Res. J.* **2004**, 22, 415.
- [22] H. Kangas, A. Suurnäkki, M. Kleen, *Nord. Pulp Pap. Res. J.* **2007**, 22, 415.
- [23] L. Forsgren, A. Venkatesh, F. Rigoulet, K. Sahlin-Sjövald, G. Westman, M. Rigdahl, A. Boldizar, *Compos. Part B Eng.* **2021**, 208, 108590.
- [24] J. Brandup, E. Immergut, E. Grulke, *Polymer Handbook*, 4th ed., John Wiley & Sons, Inc., Wiley-Blackwell **1999**.
- [25] F. B. Khambatta, F. Warner, T. Russell, R. S. Stein, *J Polym Sci Part A-2 Polym Phys* **1976**, 14, 1391.
- [26] L. Forsgren, J. Berglund, J. Thunberg, M. Rigdahl, A. Boldizar, *Polym. Eng. Sci.* **2020**, 60, 5.
- [27] J. Jiang, N. C. Carrillo-Enriquez, H. Oguzlu, X. Han, R. Bi, M. Song, J. N. Saddler, R. C. Sun, F. Jiang, *ACS Sustain. Chem. Eng.* **2020**, 8, 7182.
- [28] J. Jiang, N. C. Carrillo-Enriquez, H. Oguzlu, X. Han, R. Bi, J. N. Saddler, R. C. Sun, F. Jiang, *Carbohydr. Polym.* **2020**, 247, 116727.
- [29] N. Zhang, P. Tao, Y. Lu, S. Nie, *Cellulose* **2019**, 26, 7823.
- [30] M. Poletto, A. J. Zattera, M. M. C. Forte, R. M. C. Santana, *Bioresour. Technol.* **2012**, 109, 148.
- [31] J. R. Araújo, W. R. Waldman, M. A. De Paoli, *Polym. Degrad. Stab.* **2008**, 93, 1770.
- [32] Y. Chen, C. Xu, J. Huang, D. Wu, Q. Lv, *Carbohydr. Polym.* **2017**, 157, 303.
- [33] A. K. Townsend, H. J. Wilson, *J. Nonnewton. Fluid Mech.* **2018**, 261, 136.
- [34] V. Khoshkava, M. R. Kamal, *ACS Appl. Mater. Interfaces* **2014**, 6, 8146.
- [35] A. Sharif-Pakdaman, J. Morshedian, Y. Jahani, *J. Appl. Polym. Sci.* **2012**, 125, E305.

How to cite this article: A. Venkatesh, L. Forsgren, A. Avella, K. Banke, J. Wahlberg, F. Vilaseca, G. Lo Re, A. Boldizar, *J. Appl. Polym. Sci.* **2021**, e51615. <https://doi.org/10.1002/app.51615>